Proceedings of the ASME 34rd International Conference on Ocean, Offshore and Arctic Engineering
OMAE2015
May 31-June 5, 2015, St. John's, Newfoundland, Canada

OMAE2015-41578

TURBULENCE MODELING FOR FREE-SURFACE FLOW SIMULATIONS IN OFFSHORE APPLICATIONS

Henri J.L. van der Heiden*
Arthur E.P. Veldman†
Roel Luppes
Peter van der Plas
Institute for Mathematics and Computer Science
University of Groningen
P.O. Box 407, 9700 AK Groningen
The Netherlands
h.v.d.heiden@marin.nl
{a.e.p.veldman, r.luppes, p.van.der.plas}@rug.nl

Joop Helder
Tim Bunnik
MARIN
P.O. Box 28, 6700 AA Wageningen
The Netherlands
{j.helder, t. bunnik}@marin.nl

ABSTRACT

To study extreme hydrodynamic wave impact in offshore and coastal engineering, the VOF-based CFD simulation tool ComFLOW is being developed. Recently, much attention has been paid to turbulence modeling, local grid refinement, wave propagation and absorbing boundary conditions. Here we will focus on the design of the turbulence model, which should be suitable for the coare grids as used in industrial applications. Thereto a blend of a QR-model and a regularization model has been designed, in combination with a dedicated wall model. The QR-model belongs to a class of modern eddy-viscosity models, where the amount of turbulent eddy viscosity is kept minimal. The performance of the model will be demonstrated with several applications relevant to the offshore industry. For validation, experiments have been carried out at MARIN.

INTRODUCTION

Extreme hydrodynamic wave impact on rigid and floating structures is of high industrial interest in offshore and coastal engineering. To study the occurring phenomena the CFD VOF-based simulation tool ComFLOW has been developed; see e.g. [1–3]. In the early phase of the ComFLOW development, emphasis has been on simulating momentum-dominated phenomena, such as the impact of extreme waves (e.g. green water loading [4] and wave run-up) and on sloshing (e.g. in LNG tanks [5]). In these applications viscous effects can be mostly neglected. Later, the application area has been extended to flows where the influence of viscosity is becoming noticeable, like in side-by-side mooring or inside moonpools. Thus, recently much attention has been paid to turbulence modelling.

Numerical simulation of turbulent flow has to face the challenge of the very small spatial and temporal scales present in turbulence. A detailed description would require computational grids and time steps that resolve these small scales, which is currently not affordable. Thus strategies have been developed to model the effects of the subgrid scales onto the resolved scales: turbulence modeling through RaNS or LES models. Most of these models are eddy-viscosity models, i.e. they add an amount of 'turbulent' diffusion to the flow model to model the dissipative effect of turbulence. The drawback of the 'classical' models (like $k-\varepsilon$ or Smagorinski, including their dynamic variants), is that they often add an excessive amount of diffusion; e.g. also in laminar and transitional flow regions where they seriously disturb the physical flow phenomena.

*Present address: MARIN, P.O. Box 28, 6700 AA Wageningen, The Netherlands

†Address all correspondence to this author.

Therefore, in modern turbulence models (like WALE or sigma) the amount of turbulent diffusion is better controlled. One such method is the QR-method [6, 7]. Based on functional-analytic arguments, it estimates the unresolved subgrid-scale details, and minimizes the amount of turbulent diffusion that is added. These estimates can be described in terms of the second and third invariants, Q and R, of the rate-of-strain tensor; hence the name. This method not only recognizes laminar parts of the flow, but also whether the turbulent flow field is more or less two-dimensional (relevant near free surfaces). In regions of backscatter, the QR model is extended with a non-diffusive regularization model, which reduces the production of the smaller scales. Because in the engineering applications envisaged insufficient resolution in wall regions can be expected, a Werner-Wengle wall model is applied [8].

The behaviour of the new model will be demonstrated first on a model problem for flow past risers. Thereafter simulations of the water motion inside a moonpool will be shown, for which MARIN has performed a series of validation experiments.

THE NAVIER–STOKES EQUATIONS

The incompressible, turbulent fluid flow is modelled by means of the Navier–Stokes equations.

$$\mathscr{M}u = 0, \qquad \frac{\partial u}{\partial t} + \mathscr{C}(u)u + \mathscr{G}p - \mathscr{D}u = f. \tag{1}$$

Here $\mathscr{M}$ is the divergence operator[1] which describes conservation of mass. Conservation of momentum is based on the convection operator $\mathscr{C}(u)v = \nabla(u \otimes v)$, the pressure gradient operator $\mathscr{G} = \nabla$, the diffusion operator $\mathscr{D}(u) = \nabla \cdot \nu \nabla u$ and forcing term f. The kinematic viscosity is denoted by ν.

The Navier–Stokes equations (1) are discretized on an Arakawa C-grid. The second-order finite-volume discretization of the continuity equation at the new time level $\cdot^{(n+1)}$ is given by

$$M^0 u_h^{(n+1)} = -M^\Gamma u_h^{(n+1)}, \tag{2}$$

where M^0 acts on the interior of the domain and M^Γ acts on the boundaries of the domain. In the discretized momentum equation, convection $C(u_h)$ and diffusion D are discretized explicitly in time. The pressure gradient is discretized at the new time level. In this exposition, for simplicity reasons the first-order forward Euler time integration will be used. In the actual calculations, the second-order Adams–Bashforth method is being applied.

[1]Note that calligraphic symbols denote analytic operators, whereas their discrete counterparts will be denoted by upper-case symbols.

Taking the diagonal matrix Ω to denote the matrix containing the volumes of the control volumes, gives the discretized momentum equation as

$$\Omega \frac{u_h^{(n+1)} - u_h^{(n)}}{\delta t} = -C(u_h^{(n)})u_h^{(n)} + Du_h^{(n)} - Gp_h^{(n+1)} + f. \tag{3}$$

The discrete convection operator is skew-symmetric, i.e.

$$C(u_h^{(n)}) + C(u_h^{(n)})^T = 0, \tag{4}$$

where the superscript $\cdot^T$ denotes the transpose. In this way convection does not contribute to energy production or dissimination [9]; in particular its discretization preserves the energy of the flow and does not produce artificial viscosity. This can be seen by looking at the discrete evolution of the energy $||u_h||$:

$$\begin{aligned} \frac{\partial}{\partial t}\tfrac{1}{2}||u_h||^2 &= ((\frac{\partial}{\partial t}u_h, u_h)) = ((-C(u_h)u_h - Gp_h + Du_h, u_h)) \\ &= -((C(u_h)u_h, u_h)) - ((Gp_h, u_h)) + ((Du_h, u_h)). \end{aligned} \tag{5}$$

When the operator $C(u_h)$ is skew-symmetric, the first term in the right-hand side of (5) vanishes, i.e. no numerical diffusion is introduced. To make the discretization fully energy-preserving, the discrete gradient operator and the divergence operator are each others negative transpose, i.e. $G = -M^{0T}$, thus mimicking analytic symmetry $\nabla = -(\nabla\cdot)^T$, as in [9]. In this way, also the work done by the pressure drops out of (5).

The solution of the discrete Navier–Stokes equation is split into two steps. An auxiliary variable $\tilde{u}_h$ is defined through the equation

$$\Omega \frac{\tilde{u}_h - u_h^{(n)}}{\delta t} = -C(u_h^{(n)})u_h^{(n)} + Du_h^{(n)} + f. \tag{6}$$

Imposing discrete mass conservation (2) on the new time level $(n+1)$ results in a linear system for the pressure:

$$\delta t\, M^0 \Omega^{-1} G\, p_h^{(n+1)} = M^0 \tilde{u}_h + M^\Gamma u_h^{(n+1)}. \tag{7}$$

This equation is often referred to as the discrete pressure Poisson equation, as it can be regarded to be a discretization of the equation $\mathscr{M}\mathscr{G}p = \mathscr{M}\tilde{u}$.

The liquid region and the free liquid surface is described by an improved VOF-methid [1, 10].

TURBULENCE MODELLING

In order to simulate the high Reynolds number turbulent flows that are associated to offshore applications, some form of turbulence modeling is required. Simply put, it is necessary to model those scales of motion that cannot be represented on the computational grid, i.e. the subgrid scales. The production of small scales takes place through the non-linear convective term. The only mechanism that counteracts the production of small scales of motion is diffusion. The equilibrium between production (by convection) and dissipation (by diffusion) of small scales cannot be reached on the computational grid. This consideration gives rise to two modeling options: either restrict the production of subgrid scales or increase the dissipation of subgrid scales.

The vortex stretching mechanism

In order to arrive at a correspondence between turbulent dynamics of the fluid and the Navier-Stokes equations, consider the momentum equation. Taking the curl of equation (1) gives the evolution of the vorticity field $\omega \equiv \nabla \times u = \mathrm{curl}\, \mathrm{u}$ in time. As the curl of a gradient of a scalar field vanishes, the vorticity equation reads

$$\frac{\partial \omega}{\partial t} + \mathscr{C}(u)\omega + \mathscr{D}\omega = \mathscr{C}(\omega)u. \tag{8}$$

The term on the right-hand side describes the vortex stretching. The enstrophy of a fluid, like the kinetic energy, is defined in terms of an L_2-inner product. The enstrophy is defined as the L_2-norm of the vorticity, i.e.

$$||\omega||^2 = \int_\Omega \omega \cdot \omega \, \mathrm{d}\Omega. \tag{9}$$

Taking the inner product of (8) with the vorticity field ω and recalling the skew-symmetry of the convective term, gives an equation for the evolution of the enstrophy in time:

$$\frac{\partial ||\omega||^2}{\partial t} + ((\omega, \mathscr{D}\omega)) = ((\omega, \mathscr{C}(\omega)u)). \tag{10}$$

The vortex stretching term on the right-hand side of this equation can be written as

$$((\omega, \mathscr{C}(\omega)u)) = ((\omega, S(u)\omega)),$$

where $S(u)$ denotes the symmetric part of the velocity gradient tensor $S(u) = \frac{1}{2}(\nabla u + (\nabla u)^T)$.

When a domain Ω_Δ of arbitrary size Δ is considered, the evolution of enstrophy in this domain is governed by (10), which is written as

$$\frac{\mathrm{D}||\omega||^2_\Delta}{\mathrm{D}t} = \int_{\Omega_\Delta} \omega \cdot S(u)\omega + \nu\omega \cdot \nabla^2\omega \, \mathrm{d}\Omega. \tag{11}$$

Both terms in the right-hand side are closely related to invariants of the rate-of-strain tensor. In the absence of boundary terms, the diffusive term in (11) can be rewritten as

$$((\omega, \nabla^2\omega))_\Delta = -((\nabla\omega, \nabla\omega))_\Delta = \int_{\Omega_\Delta} \mathrm{tr}\, S^2(\omega) \, \mathrm{d}\Omega, \tag{12}$$

where $S(\omega) = \frac{1}{2}(\nabla\omega + (\nabla\omega)^T)$ denotes the symmetric part of the vorticity gradient tensor. Note that the right-hand side of this equation equals the second invariant of the tensor $S(\omega)$, given by

$$q(\omega) \equiv \tfrac{1}{2}\mathrm{tr}\, S^2(\omega).$$

As has been demonstrated by Chae [11] in an analysis of the 3-D Euler equations, the vortex stretching term can be expressed in terms of the third invariant of the rate-of-strain tensor. The third invariant $r(u)$ of the strain-rate tensor $S(u)$ is defined as

$$r(u) \equiv \tfrac{1}{3}\mathrm{tr}\, S^3(u) = \det S(u). \tag{13}$$

The computations of Chae [11] show that $r(u)$ is related to the vortex stretching term by the following expression

$$\int_{\Omega_\Delta} r(u) \, \mathrm{d}\Omega = \int_{\Omega_\Delta} \omega \cdot S(u)\omega \, \mathrm{d}\Omega,$$

which allows to rewrite (11) describing the evolution of the enstrophy as

$$\frac{\mathrm{D}||\omega||^2_\Delta}{\mathrm{D}t} = \int_{\Omega_\Delta} (r(u) - \nu q(\omega)) \, \mathrm{d}\Omega. \tag{14}$$

This relation is important in analyzing and formulating the turbulence models that will be described below.

LARGE-EDDY MODELS

The Smagorinsky model

An important class of LES turbulence models relies on the turbulent viscosity hypothesis, e.g. [12]. An eddy viscosity model defines the effect of subfilter scales on the resolved scales

as a locally increased diffusivity of the flow. In an eddy viscosity model, it is assumed that the anisotropic part of the subfilter tensor is proportional to the filtered rate-of-strain tensor $S(\bar{u})$, i.e.

$$\tau - \tfrac{1}{3}(\mathrm{tr}\,\tau)I = -2\nu_{ed}S(\bar{u}),$$

where the constant of proportionality ν_{ed} is dubbed the eddy viscosity. The trace of the subfilter tensor $\mathrm{tr}\,(\tau)$ can be incorporated into the pressure. The archetype of eddy-viscosity LES models is the Smagorinsky model, first formulated in 1963 by Joseph Smagorinsky [13]. The Smagorinsky eddy viscosity is assumed to be proportional to the local stresses in the fluid. The characteristic stress $|S(\bar{u}|$ is related to the second invariant of the rate-of-strain tensor q through $|S(\bar{u})|^2 = \mathrm{tr}\,S^2(\bar{u}) = q(u)$. The Smagorinsky eddy viscosity is obtained from multiplying the characteristic stress by a turbulent mixing length or filter length. If $\bar{\Delta}$ denotes the filter length, the Smagorinsky eddy viscosity is given by

$$\nu_{ed} \equiv C_S\bar{\Delta}^2|S(\bar{u})|, \tag{15}$$

where C_S denotes the Smagorinsky coefficient, which has to be determined empirically. Typically a value in the range of 0.1-0.18 is used for C_S. Note furthermore that the resulting continuity and momentum equations are written only in terms of the filtered velocity field $\bar{u}$, which shows that in the Smagorinsky model there is no need to perform an explicit filter operation in the course of the computation to determine the filtered velocity field.

The transfer of energy from resolved to subfilter scales according to the Smagorinsky model is found to be $P_s = \nu_{ed}|S(\bar{u})|^2$, which is clearly always nonnegative. This shows that dissipation is enhanced in regions of high rates-of-strain. Note that energy dissipation will also occur in laminar parts of the flow, where, e.g., only a shear layer is present. This is an undesirable feature of the Smagorinsky model, and some modifications have been proposed, e.g. a dynamic version which adapts to the local flow physics [14, 15].

QR eddy-viscosity model

In order to overcome unnecessary and excessive dissipation in a turbulent flow, an answer to the question "When does eddy-viscosity damp subfilter scales sufficiently?" is sought. Starting from this question, Verstappen [6] arrives at the QR eddy-viscosity model. One of the ways through which he arrives at model is by way of a classical analysis of the vortex stretching mechanism that has been presented above. Adding an eddy-viscosity term to the Navier-Stokes equations, allows a derivation of the enstrophy evolution equation (14) as

$$\frac{\mathrm{D}||\omega||^2_\Delta}{\mathrm{D}t} = \int_{\Omega_\Delta} (r(u) - (\nu + \nu_{ed})q(\omega))\,\mathrm{d}\Omega. \tag{16}$$

Therefore, in order to counteract the vortex stretching beyond the scale $\bar{\Delta}$, it is sufficient to demand that

$$\nu_{ed}\int_{\Omega_\Delta} q(\omega)\,\mathrm{d}\Omega \geq \int_{\Omega_\Delta} r(u)\,\mathrm{d}\Omega.$$

Using Poincaré's Lemma, the left hand side of the equation can be estimated as

$$\nu_{ed}\int_{\Omega_\Delta} q(\omega)\,\mathrm{d}\Omega \geq \frac{\nu_{ed}}{C_\Delta}\int_{\Omega_\Delta} q(u)\,\mathrm{d}\Omega,$$

where C_Δ is the smallest nonzero eigenvalue of the Laplacian operator ∇^2 on the domain Ω_Δ. In a numerical implementation, this eigenvalue will be based on the local computational grid information. The result gives an eddy viscosity model that is entirely based on the invariants q and r of the rate-of-strain tensor:

$$\nu_{ed} = C_\Delta \frac{\int_{\Omega_\Delta} r(u)\,\mathrm{d}\Omega}{\int_{\Omega_\Delta} q(u)\,\mathrm{d}\Omega}. \tag{17}$$

In order to evaluate the eddy-viscosity in the course of computation, note that the integrals in the last expression can be interpreted as a filter applied to the invariants of the rate-of-strain tensor. Using the approximate deconvolution method to regain subfilter information, Verstappen [6] shows that to second order in the filter length $\bar{\Delta}$ an appropriate estimate for the integrals in equation (17) yields the QR eddy-viscosity as

$$\nu_{ed} = \frac{4}{\bar{\Delta}}\frac{r(u)}{q(u)}. \tag{18}$$

Note that the calculation of the invariants in (18) requires only algebraic manipulations, and does not noticeably add to the total CPU-cost of the simulations.

It is remarked that the sign of the third invariant $r(u)$ might become negative. Physically interpreted, a positive value of the invariant r corresponds to the transfer of energy from resolved to subfilter structures, i.e. the forward energy cascade. A negative value of r corresponds to the anti-diffusive transfer of energy from subfilter to resolved scales. As the eddy viscosity hypothesis was intended to model the forward energy cascade, the possibility of a negative value of r is undesirable. A clipping procedure can take care of the positivity of the eddy viscosity, and ensure a computationally stable algorithm. Defining $r_+ = \max(r,0)$, the resulting eddy viscosity model is given by replacing r by r_+. Nevertheless, in the course of computing a turbulent flow, situations in which $r < 0$ might occur, indicating a production of energy on the smallest resolvable scales. The complete computational and numerical model should be closed also

for occurrences of negative r, though preferably not by an eddy viscosity model. This will introduce an unphysical dissipation of energy. Rather, the creation of energy on filter scales should be prevented through a modification of the convective term.

The QR-model has been extensively tested on a number of 'elementary' flows like decaying isotropic turbulence [16] and channel flow [6, 17]. Comparisons with the popular dynamic version of the Smagorinsky model [15] can be found in [16, 18]. Especially [18] gives a good comparison, because there exactly the same grid and the same numerical method are used for both models, so that numerical discretization errors do not hamper the comparison. It is found that the behaviour of the QR-model on the smaller length scales is clearly better because of the reduced dissipation.

Regularization of convection

Preventing the vortex stretching mechanism from creating scales of motion that cannot be resolved can be achieved by a regularization of the convective term. The first approach in this direction has been Leray's smoothing of the advection-velocity [19], followed more recently by the Navier-Stokes α-model, in which effectively the transported momentum velocity is smoothed [20]. The third type of regularization, due to Verstappen [21], regularizes the convective term in an explicit symmetry-preserving way, unlike the other regularization approaches.

A symmetry-preserving regularization of the convective term smoothes the original convective term while preserving its skew-symmetry. The smoothing takes place through a filter operation $u_h \rightarrow \overline{u_h}$. Verstappen [21] applies the filter to the convective term, which yields a family of symmetry-preserving regularization models. For the discrete convective term $C(u_h)u_h$, the second-order (in terms of the filter length) accurate regularization model from this family is given by

$$C_2(u_h,u_h) = \overline{C(\overline{u_h})\,\overline{u_h}}. \tag{19}$$

Selfadjointness of the filter ensures the skew-symmetry of the original convective term. The length scale over which the filter smoothes the signal will depend on the local flow physics.

In the regularization approach, the filter width $\bar{\Delta}$ can possess different optimal values for changing flow configurations, see the simulations presented in [23]. Stopping the vortex stretching mechanism at grid scales provides the key to determining the optimal value for the filter width $\bar{\Delta}$. The equivalent of the enstrophy equation (10) in the regularization context reads

$$\frac{\partial ||\omega||^2}{\partial t} + ((\omega, \mathscr{D}\omega)) = ((\omega.\mathscr{C}_2(\omega)u)).$$

In order to restrain the dynamics of resolvable scales motion to scales $> \bar{\Delta}$, which concerns wave modes $|k| < k_c$ where $k_c = \pi/\bar{\Delta}$. In order to restrain the dynamics to scales $> \Delta$, it should hold that $\frac{\partial ||\omega||^2_{\bar{\Delta}}}{\partial t} \leq 0$. Recalling the enstrophy equation in terms of the invariants of the rate of strain tensor (14) and Poincaré's Lemma, gives the condition for restraining the dynamics to resolvable scales of motion as

$$|r(u)| \geq \frac{\nu}{C_\Delta} q(u) \geq f_2(\Delta)|r(u)|,$$

where $f_2(\bar{\Delta})$ is the damping factor. The first ineuality should hold, as otherwise there is no need to filter. Therefore, $f_2(\bar{\Delta})$ is restricted to

$$f_2(\bar{\Delta}) = \min\left(1, \frac{\nu}{C_\Delta}\frac{q(u)}{|r(u)|}\right).$$

Given a discrete filter, if the equality sign holds, then this condition implies a filter length [22].

A blending strategy

In both RaNS and LES approaches to turbulent flow simulation, the purely dissipative turbulent and eddy viscosity models allow the flow to reach an equilibrium between energy production and dissipation on the computational grid. Generically, the energy dissipation is enhanced at scales of motion that are well-resolved. Thereby the convective production of small scales of motion is prevented and the eddy/turbulent viscosity models the continuation the forward energy cascade beyond the grid scale.

Another perspective is given by the regularization approach, in which the diffusive term is left unaltered. In the parameter-free regularization model, the filter width is locally adjusted to prevent the creation of subgrid scales of motion through the process of vortex stretching. As a result, the regularization approach does not interfere with any physical process up to the scale set by the computational grid. At the grid scale a filter operation prevents the convective term from producing smaller scale structures.

The interaction of resolved scales of motion with subfilter scales of motion are quantified by the third invariant $r(u)$ of the rate-of-strain tensor. For positive values of r, the equations of motion suggest that energy is transferred from large to small scales of motion, and a suitable model seems to be the QR eddy-viscosity model. However, when a negative value of r occurs, this indicates a transfer of energy from subfilter to resolved scales of motion. This backscatter of energy is not allowed by the requirement that the dynamics of resolved and unresolved scales should be completely separated. A negative value of r would introduce anti-diffusive behavior of the QR eddy-viscosity model. This suggests that the model can be closed for

backscatter through regularization of the convective term. The suggested approach blends two different modeling approaches into one blended turbulence model, depending on the invariants of the rate-of-strain tensor.

The near-wall boundary layer

From a computational point of view it is undesirable to refine the grid to the level at which the boundary layer can be resolved. Therefore, to account for the influence of the turbulent boundary layer on the effective wall-shear stress that the outer flow experiences, some form of wall modeling has to be applied. Hereto, the Werner–Wengle model has been selected [8].

SIMULATION RESULTS

Wake behind a square cylinder

The first example of the performance of the turbulence model concerns the flow past a square cylinder at Re=22,000. Although its cross section is square, it can be considered as a first model for simulating turbulent wakes, like in the flow past risers (although the Reynolds number is about two orders of magnitude larger). This flow case has been the subject of a series of workshops, where various turbulence models and discretization schemes have been compared [27]. Thus, much reference material is available to assess the performance of the present simulation model.

The problem is defined in a rectangular domain: $x \in [-5,15]$, $y \in [-7,7]$, $z \in [0,4]$, with the unit-square cylinder centered around $(x,y) = (0,0)$. The oncoming flow is uniform with unit velocity. On the top and bottom walls a slip boundary condition is prescribed, whereas the flow is periodic in the span wise direction. A snapshot (on a very fine grid) of the vortex formation behind the cylinder is given in Fig. 1. It shows the small length scales of the flow, which form a challenge for any turbulence model.

The reference material from the previous workshops is summarized in Fig. 2. It shows the results for the drag coefficient for a large number of simulation methods. The convective discretization determines the outcome more than the choice of the model, which is shown in the top graph of Fig. 2. In the bottom graph (most of) the LES-results have been ordered in terms of their discretization: *U* stands for upwind, and *C* for a central discretization. The experimental results of Lyn *et al.* [24], Lee [25] and Vickery [26] fall within the demarcated area. The results of the large-eddy simulations are taken from Rodi [27] and Voke [28]. Although these resultas are almost two decades old, they are still useful to illustrate the influence of numerical dissipation. The differences in the results are clearly more determined by the numerical diffusion (observe how the upwind results in Fig. 2 group together), than by the selected turbulence model. The only upwind results in this graph that are close to

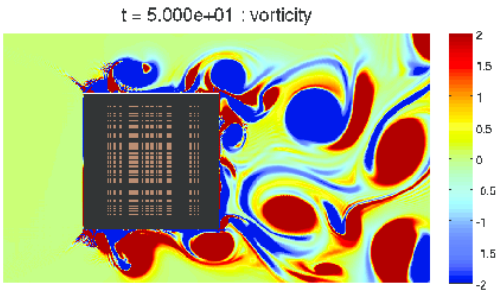

FIGURE 1. SNAPSHOT ON A FINE GRID AT $t = 50s$ OF THE VORTICES CLOSE TO THE CYLINDER¡ GIVING AN IMPRESSION OF THE SMALL LENGTH SCALES PRESENT IN THE FLOW.

the experiment (see U5) are from an extremely fine fifth-order calculation. The C4-result in Fig. 2 is from a fourth-order version of the current symmetry-preserving discretization [9], without a further turbulence model. Thus, in ComFLOW we opt for a symmetry-preserving discretization scheme, which does not produce any numerical diffusion. The grid will be much coarser, however, than in [9], which forms an engineering challenge.

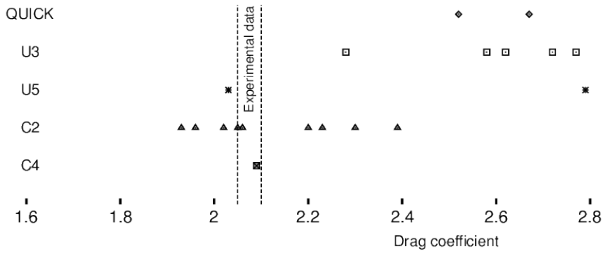

FIGURE 2. THE MEAN DRAG COEFFICIENT FOR FLOW PAST A SQUARE CYLINDER AT Re $= 22,000$ FOR VARIOUS LES-MODELS ORDERED BY THE DISCRETIZATION OF THE CONVECTIVE TERM (STATUS IN 1997).

The grids in the ComFLOW simulations are not fine enough for 'real' DNS resolution, and maybe not even fine enough for a 'physical' LES simulation. In underresolved simulations, a LES model has more the task to suppress numerical wiggles (because the grid is too coarse to catch the solution) than to model subgrid-scale physics (because the grid is too coarse to catch the physics). There is a gliding scale, from coarse towards fine grids, where first the model acts 'numerically', and later it acts 'physically'. Ultimately, when the grid is fine enough to resolve all flow details, the model should switch itself off. The QR-model is designed to cover this whole range without the need for any additional numerical dissipation. It is now interesting to find out

in practical calculations how QR and other turbulence models are able to keep the 'model inaccuracy' within limits.

Several turbulence models have been tried, to study the influence of these models on the results. The first model is 'no model', i.e. a symmetry-preserving central discretization without any numerical diffusion [9]. It is compared with the Smagorinsky model, explained in (15), in combination with the symmetry-preserving discretization in order not to interfere with the turbulence model. Finally, the blended QR-model (18) has been applied, again with the symmetry-preserving discretization. An overview of the results for the drag coefficient as a function of the number of grid points is given in Figure 3. On the coarser grids the Smagorinski model gives the lowest drag, whereas 'no model' looks the best. On the finer grids the models agree more with each other, with 'no model' being the inferior. It appears that the QR-model could be a useful compromise. It is good to realize that these grids with around 100,000 grid points are much coarser than the ones used in Fig. 2, where typically 10 million (or more) grid points have been used. More grid refinement studies are needed to further identify the stronger and weaker aspects of the various models.

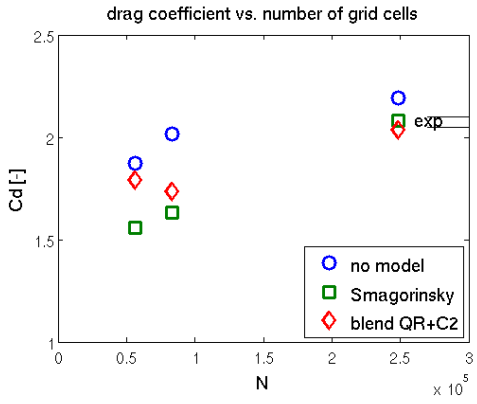

FIGURE 3. COMPUTED DRAG COEFFICIENT FOR FLOW PAST A SQUARE CYLINDER AT Re $= 22,000$ FOR SEVERAL TURBULENCE MODELS AND NUMBER OF GRID POINTS (N).

Moonpool water motion

The simulation of free-surface dynamics in moonpools is an example of an application where violent free-surface motion is coupled to viscous flow details. A realistic simulation of free-surface motion is strongly dependent on the correct prediction of the vortex formation in the moonpool. The combination of coarse grids and upwind discretization techniques dissipates the perturbations that lead to the characteristic roll-up of the shear layer, thus preventing vortex formation at the edges of the moonpool.

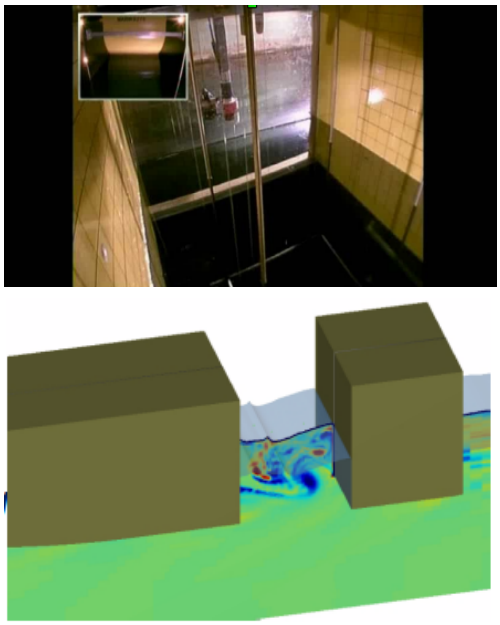

FIGURE 4. TOP: PHOTOGRAPH OF THE MOONPOOL EXPERIMENT. BOTTOM: SNAPSHOT OF THE SIMULATION SHOWING VORTEX SHEDDING.

In order to illustrate the performance of the above-described central discretization, the first results of the simulation of water motion in a moonpool (in calm water) will be presented. The experimental set-up at MARIN is shown in Fig. 4, together with a snapshot from the numerical simulations. The experimental set-up has been designed such that the flow stays as two-dimensional as possible, such that flow structures in spanwise direction do not contribute significantly to the global flow dynamics.

In order to model moonpool dynamics in calm water (i.e. in the absence of waves) not the entire ship will be modeled. The domain has dimensions (in m) $[5.0, 6.0] \times [0.5, 0.5] \times [4.0, 0.5]$, and the stretched grid has dimensions $228 \times 10 \times 184$. As the setup of the problem is two-dimensional and most variation is expected to take place in the (x,z)-plane, we assume that 10 uniformly spaced grid points in the are y-direction are enough to capture the essential physics. The smallest grid spacing is $0.01m$.

In rest, the flat free-surface $(z = 0)$ is elevated $0.4m$ above the submerged bottom of the object, i.e. the draft is taken to be $0.4m$ The width of the moonpool is $0.8m$ in stream-wise (x) direction and $1.0m$ in cross-stream (y) direction. Rather than moving the moonpool through the grid or to prescribe the inflow velocity, the moonpool and the grid fixed to the geometry are accelerated from rest. The acceleration is modeled through the forcing term in the Navier–Stokes equations. No-slip boundary conditions are applied at all the moonpool walls.

The moonpool is accelerated to two constant speeds: $0.7m/s$ and $1.0m/s$. The evolution of the water motion in the moonpool

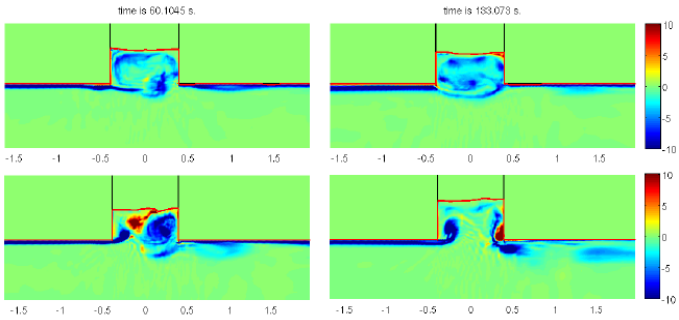

FIGURE 5. DEVELOPMENT OF VORTICITY IN TIME (FROM LEFT TO RIGHT: 60 s AND 133 s) FOR A FINAL SPEED (AFTER ACCELERATION) OF 0.7 m/s (TOP) AND 1.0 m/s (BOTTOM).

is illustrated by the vorticity plots in Fig. 5. In the first stage, during acceleration of the moonpool a big vortex is formed at the edge and shear layer roll-up is observed. The vortex travels upward in the moonpool and impinges on the free surface. For the lower speed $(0.7m/s)$ the vortices that are formed at the edge circulate through the moonpool, deforming the free surface and inducing a small-amplitude oscillation of the water column (the piston mode). For the higher speed $(1.0m/s)$, the elevation of the free-surface is more dramatic, which can clearly be seen from the oscillation of the water height in Fig. 6. The synchronization of vortex formation and the oscillation of the water column lead to resonant (piston mode) motion of the water in the moonpool. Moreover, a bore formed by the impinging vortex on the right-side wall of the moonpool is observed to travel back and forth between the right and left wall (slosh mode).

The spectrum of the water height in the middle of the moonpool (time series) is compared in Fig. 7. A very good agreement is obtained between experiment and simulation. This also is visible in the comparison of a detailed window of the time series in Fig. 8: both amplitude and phase velocity look pretty similar.

These results are a clear improvement over a second-order upwind discretization which results in a steady state solution, with a stationary recirculation zone present in the moonpool (see the discussion in [29]). Also, traditional LES models (like the Smagorinsky model) produce a more diffusive flow pattern, with much less vortical details. It pays off that the current blended turbulence model is minimizing the amount of eddy viscosity. We hope to present a detailed comparison between the results from various turbulence models in the near future.

CONCLUSIONS

The turbulence modeling in the free-surface flow solver COMFLOW with the QR-model has been demonstrated and discussed. A first impression of its potential and performance has been presented. The QR turbulence model belongs to a modern

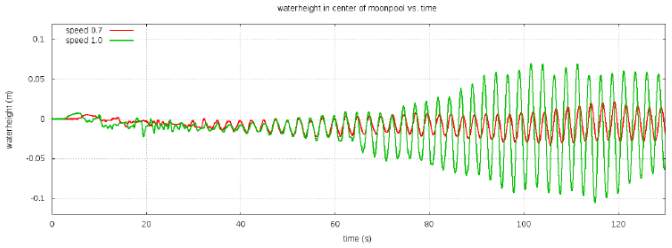

FIGURE 6. WATER HEIGHT AS A FUNCTION OF TIME FOR THE TWO FINAL SPEEDS (AFTER ACCELERATION) IN THE SIMULATION. FOR THE WATER MOTION AT FINAL SPEED $1.0m/s$ RESONANCE BEHAVIOUR IS OBSERVED.

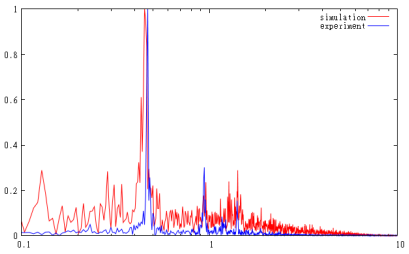

FIGURE 7. EXPERIMENT vs SIMULATION: SPECTRUM OF THE WATER HEIGHT IN THE MIDDLE OF THE MOONPOOL. NOTE THAT THE RESONANCE FREQUENCY IS QUITE NICELY CAUGHT IN THE SIMULATIONS.

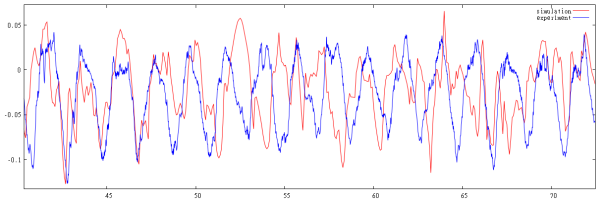

FIGURE 8. EXPERIMENT vs SIMULATION: PART OF A TIME TRACE OF THE WATER HEIGHT IN THE MIDDLE OF THE MOONPOOL AS A FUNCTION OF TIME. NOTE THAT THE AMPLITUDES ARE QUITE COMPARABLE.

class of models, where turbulent eddy viscosity is kept to a minimum. It has been extended with a (dissipation-free) regularization model, to deal with backscatter. The performance of the new model has been demonstrated first on flow past a square cylinder. Thereafter, its performance on simulating flow in a moonpool has been discussed, for which validation experiments have been carried out at MARIN. Especially its behaviour on 'engineering grids', i.e. grids that are deemed too coarse for the traditional turbulence models, has been assessed. A more elaborate discussion will follow in the PhD-thesis by the first author, which will be published shortly.

ACKNOWLEDGMENT

This research is supported by the Dutch Technology Foundation STW, applied science division of NWO and the technology programme of the Ministry of Economic Affairs in The Netherlands (contracts GWI.6433 and 10475).

REFERENCES

[1] Kleefsman, K.M.T., Fekken, G., Veldman, A.E.P., Iwanowski, B., and Buchner, B., 2005. "A volume-of-fluid based simulation method for wave impact problems". *Journal of Computational Physics*, **206**(1), pp. 363–393.

[2] Veldman, A.E.P., Luppes, R., Bunnik, T., Huijsmans, R.H.M., Düz, B., Iwanowski, B., Wemmenhove, R., Borsboom, M.J.A., Wellens, P.R., van der Heiden, H.J.L., and van der Plas, P., 2011. "Extreme wave impact on offshore platforms and coastal constructions". In *30th Conf. on Ocean, Offshore and Arctic Eng. OMAE2011*, Rotterdam (The Netherlands), 19-24 June 2011, paper OMAE2011-49488.

[3] Veldman, A.E.P., Luppes, R., van der Heiden, H.J.L., van der Plas, P., Düz, B. and Huijsmans, R.H.M., 2014. "Turbulence modeling, local grid refinement and absorbing boundary conditions for free-surface flow simulations in offshore applications". *33rd Int. Conf. on Ocean, Offshore and Arctic Engng*, San Francisco, 8-13 June, 2014. Paper OMAE2014-24427.

[4] Fekken, G., Veldman, A.E.P. and Buchner, B., 1999. "Simulation of green-water loading using the Navier-Stokes equations". In J. Piquet (ed.) *Proceedings 7th International Conference on Numerical Ship Hydrodynamics*, Nantes (France), 19-22 July 1999, paper 12.

[5] Wemmenhove, R., Luppes, R. and Veldman, A.E.P., 2008. "Application of a VOF method to model compressible two-phase flow in sloshing tanks". *27th Conference on Offshore Mechanics and Arctic Engineering OMAE Conference*, Estoril (Portugal), 16-19 June 2008, paper OMAE2008-57254.

[6] Verstappen, R.W.C.P., 2011. "When does eddy viscosity damp subfilter scales sufficiently?" *Journal of Scientific Computing*, **49**(1), pp. 94–110.

[7] Verstappen, R.W.C.P., 2013. "Blended scale-separation models for large eddy simulations". In *Proceedings 14th European Turbulence Conference ETC14*, Lyon (France), September 1-4.

[8] Werner, H. and Wengle, H., 1993. "Large-eddy simulation of turbulent flow over and around a cube in a plate channel". In *8th Symposium on Turbulent Shear Flows*. SpringerVerlag, pp. 155–168.

[9] Verstappen, R.W.C.P. and Veldman, A.E.P., 2003. "Symmetry-preserving discretization of turbulent flow". *Journal of Computational Physics*, **187**, pp. 343–368.

[10] Hirt, C.W. and Nichols, B.D., 1981. "Volume of fluid (VOF) method for the dynamics of free boundaries". *Journal of Computational Physics*, **39**, pp. 201–225.

[11] Chae, D., 2005. "On the spectral dynamics of the deformation tensor and new a priori estimates for the 3-D Euler equations". *Commun. Math. Phys.*, **263**, pp. 789–801.

[12] Sagaut, P., 2001. "*Large Eddy Simulation for Incompressible Flows*". Springer-Verlag.

[13] Smagorinsky, J., 1963. "General circulation experiments with primitive equations". *Monthly Weather Review*, **91**(3), pp. 99–183.

[14] Germano, M., Piomelli, U., Moin, P. and Cabot, W.H., 1991. "A dynamic subgrid-scale eddy viscosity model". *Physics of Fluids A*, 3(7), pp. 1760–1765.

[15] Lilly, D.K., 1992. "A proposed modification of the Germano subgrid scale closure method". *Physics of Fluids A*, 4, 633–635.

[16] Verstappen, R.W.C.P., Bose, T.S., Lee, J., Choi, H. and Moin, P., 2010. "A dynamic eddy-viscosity model based on the invariants of the rate-of-strain." *Proc. Summer Program 2010*, Center for Turbulent Research, Stanford University, pp. 183–192.

[17] Rozema, W., Kok, J.C., Verstappen, R.W.C.P., and Veldman, A.E.P. , 2014. "A symmetry-preserving discretization and regularization model for compressible flow with application to turbulent channel flow." *Journal of Turbulence*, 15(6), pp. 386–410.

[18] Verstappen, R.W.C.P., Rozema, W. and Bae, H.J., 2014. "Numerical scale separation in large-eddy simulation." *Proc. Summer Program 2014*, Center for Turbulent Research, Stanford University, pp. 417–426.

[19] Leray, J., 1934. "Sur le mouvement d'un liquide visqueaux emplissant l'espace." *Acta Mathematica*, **63**, pp. 193–248.

[20] Geurts, B.J. and Holm, D., 2003. "Regularization modeling for large-eddy simulation". *Physics of Fluids*, **15**, pp. L13-L16.

[21] Verstappen, R.W.C.P., 2008. "On restraining the production of small scales of motion in a turbulent channel flow". *Computers and Fluids*, **37**(7), pp. 887–897.

[22] Trias, F.X. and Verstappen, R.W.C.P., 2011. "On the construction of discrete filters for symmetry-preserving regularization models". *Computers and Fluids*, **40**(1), pp. 139–148.

[23] Trias, F.X., Verstappen, R.W.C.P., Gorobets, A., Soria, M. and Oliva, A., 2010. "Parameter-free symmetry-preserving regularization modeling of a turbulent differentially heated cavity". *Computers and Fluids*, **39**(10), pp. 1815–1831.

[24] Lyn, D.A., Einav, S., Rodi, W. and Park, W.H., 1995. "A laser-Doppler-velocimetry study of emsemble-averaged characteristics of the turbulent near wake of a square cylinder". *J. Fluid Mech.* **304**, pp. 285–316.

[25] Lee, B.A., 1975. "The effect of turbulence on the surface

pressure field of square prisms". *J. Fluid Mech.*, **69**, pp. 263–282.

[26] Vickery, B.J., 1966. "Fluctuating lift and drag on a long square cylinder of square cross-section in a smooth and in a turbulent stream". *J. Fluid Mech.,* **25**, pp. 481–494.

[27] Rodi, W., Ferziger, J.H., Breuer, M. and Pourquié, M., 1997. "Status of large-eddy simulation: results of a workshop". *ASME Journal of Fluids Engineering*, **119**, pp. 248–262.

[28] Voke, P.R., 1997. "Flow past a square cylinder: test case LES2". In: J.P. Chollet *et al.* (eds.), *Direct and Large Eddy Simulation II*, pp. 355–373.

[29] Gaillarde, G. and Cotteleer, A., 2005. *"Water motion in moonpools: empirical and theoretical approach"*. Technical report, Maritime Research Institute Netherlands (MARIN), HMC Heerema.